The Astronomical Journal, 159:72 (8pp), 2020 February https://doi.org/10.3847/1538-3881/ab5f5d

Very Long Baseline Array Astrometry of *Cassini*: The Final Epochs and an Improved Orbit of Saturn

Dayton L. Jones[1], William M. Folkner[2], Robert A. Jacobson[2], Christopher S. Jacobs[2], Jonathan Romney[3], and Vivek Dhawan[4]
[1] Space Science Institute, 4750 Walnut Street, Suite 205, Boulder, CO 80301, USA; djones@spacescience.org
[2] Jet Propulsion Laboratory, California Institute of Technology, 4800 Oak Grove Drive, Pasadena, CA 91109, USA
[3] Long Baseline Observatory, P.O. Box 0, 1003 Lopezville Road, Socorro, NM 87801, USA
[4] National Radio Astronomy Observatory, P.O. Box 0, 1003 Lopezville Road, Socorro, NM 87801, USA
Received 2019 May 28; revised 2019 December 3; accepted 2019 December 4; published 2020 January 28

Abstract

We report results from multi-epoch radio astrometry of the *Cassini* spacecraft with the Very Long Baseline Array (VLBA). These observations are part of a program to determine a series of accurate positions for the Saturn system barycenter in the inertial International Celestial Reference Frame (ICRF) and to use these position measurements to improve our knowledge of Saturn's orbit in the planetary ephemeris. Our VLBA observations cover the full duration of the orbital phase of the *Cassini* mission, from Saturn orbit insertion in 2004 to the end of mission in 2017. This period covers more than one-third of Saturn's orbital period, allowing us to obtain good orbit constraints for Saturn, particularly on the inclination and ascending node longitude. During the early years of *Cassini*'s orbital mission our VLBA data dominated the determination of orbit orientation, while later in the mission range measurements become more significant. The orientation of Saturn's orbit is now known to approximately 0.25 milli-arcseconds (1.25 nrad), an order of magnitude improvement since the start of *Cassini* observations. Continuing improvements in the ICRF position accuracy for our phase reference sources, and possible improvements in the final orbit solutions for *Cassini*, may lead to a still better Saturn orbit over the coming years.

Unified Astronomy Thesaurus concepts: Radio astrometry (1337); Ephemerides (464); Saturn (1426)

1. Introduction

The planetary ephemeris provides a model for the positions and motions of objects in our solar system that can be used for a wide variety of applications, such as interplanetary spacecraft navigation (Melbourne 1976), dynamical studies and tests of gravitational theories (Hees et al. 2015), predictions of transits, eclipses, and occultations, and the analysis of pulsar timing observations (Lazio et al. 2017). An ephemeris is created by integrating the equations of motion for solar system bodies using a large set of observational data for initial conditions and dynamical constraints (Standish & Williams 2006). These data include historical optical observations, more recent and accurate astrometric measurements, planetary radar ranges, and spacecraft tracking of planetary flybys, orbiters, and landers. Radio interferometry (Sovers et al. 1998; Thompson et al. 2017) combined with range measurements (Konopliv et al. 2006; Shin et al. 2014) provide the most accurate positional data for spacecraft, which can be transferred to planetary positions if the trajectory of the spacecraft with respect to the planet is known. In general, astrometric measurements provide the strongest constraints on orbital inclination and ascending node, while range measurements provide the best constraints on orbital semimajor axis and eccentricity.

We have used the *Cassini* spacecraft during its 13 yr orbital mission about Saturn (2004–2017) to produce a series of high-accuracy positions for the barycenter of the Saturn system, based on astrometry of the *Cassini* 8.4 GHz downlink signal with radio interferometry. Similar observations of Mars orbiters (Park et al. 2015) and continuing observations of the Juno spacecraft orbiting Jupiter (Jones et al. 2018) all contribute to improvement of the planetary ephemeris.

2. Observations

The technique of very-long-baseline interferometry (VLBI) combines recorded signals from widely separated radio telescopes to provide high angular resolution imaging and high-precision astrometry. The most precise astrometry is based on the phase delay between pairs of radio telescopes, but there are potential cycle ambiguities in phase delays. These ambiguities can be eliminated using group delays instead, but this is an intrinsically less precise observable. One way to use the full precision of phase delays is to make narrow-angle measurements of the position differences between angularly nearby radio sources. Most systematic errors scale with the angular separation between sources, and for separations of a few degrees or less it is possible to remove cycle ambiguities from differential phase delay measurements. The position of the spacecraft can be determined with submilliarcsecond precision with respect to the a priori position of the reference source (Lestrade et al. 1990; Guirado et al. 2001; Fomalont 2006).

Phase delays are more sensitive to radio core position shifts, and there is some additional error in combining differential position offsets determined from phase delays with reference source positions determined from group delays. However, the difference in phase delay versus group delay core shift effects is at the level of 0.1 mas (Porcas 2009), which is smaller than our measurement error.

The observations and results presented here were obtained with the Very Long Baseline Array (VLBA),[5] a dedicated ten-telescope array dedicated to VLBI observations (Napier 1995). We scheduled observing epochs a few times per year during

[5] https://science.nrao.edu/facilities/vlba

Table 1
Summary of Observing Epochs, Phase Reference Sources, Typical Correlated Flux Densities on 5000 km Baselines,[a] and the Angular Separation between *Cassini* and the Reference Source

Epoch	VLBA Code	Phase Reference Source	Long Baseline Flux Density (mJy)	Angular Sep. (deg)
2014 Jul 23	BJ082A	J1502–1508	90	1.1
2014 Sep 15	BJ082B	J1508–1548	270	0.3
2015 Jan 25	BJ082C	J1608–1625	80	2.4
2015 Mar 9	BJ082D	J1617–1941	140	1.3
2015 Sep 20	BJ082F	J1551–1755	~80	0.7
2015 Nov 20	BJ082G	J1617–1941	140	0.2
2016 Jan 4	BJ082H	J1642–2007	140	0.6
2016 Jun 9	BJ085A	J1642–2007	140	0.8
2017 Mar 15	BJ085F	J1742–1517	100	6.9
2017 Jun 23	BJ085H	J1709–1728	270	7.0
2017 Sep 10	BJ085J	J1700–2610	400	6.3

Note.
[a] Flux densities from http://www.vlba.nrao.edu/astro/calib/vlbaCalib.txt and http://www.vlba.nrao.edu/cgi-bin/vlba_calib.cgi. Note that compact radio sources are often variable.

periods when an adequately strong and compact extragalactic radio source was available within a few degrees of *Cassini*'s position to use as a reference for differential phase measurements, and when *Cassini* was transmitting to one of the Deep Space Network spacecraft tracking antennas at Goldstone, California. The sky coverage from Goldstone is similar to that of central antennas of the VLBA.

Our observations were all made at 8.4 GHz, the *Cassini* downlink frequency compatible with available VLBA receivers. Prior to 2015 we used a total recording bandwidth of 256 Gb s^{-1}, divided into four intermediate frequency (IF) bands using right-hand circular polarization (RCP; *Cassini* transmits with RCP only). Each IF band was 8 MHz wide and divided into 256 spectral channels during correlation. The four IF bands were spaced unevenly, with typical center frequencies of 8428, 8500, 8790, and 8890 MHz. This improved multiband (group) delay resolution.

Since 2015 we used a total recording bandwidth of 2 Gb s^{-1}, divided into eight pairs of dual-polarization IF bands. Each of the 16 IF bands had a bandwidth of 32 MHz, digitized at 64 Msamples/s with 2 bits/sample. The correlator provided 128 spectral channels per IF, giving a channel resolution of 250 kHz. This allowed several spectral channels across the bandwidth of the *Cassini* downlink signal. Our total observing band was 8272–8528 MHz, still adequate for good multiband delay resolution.

Each observing epoch was 4 hr long, with alternating short scans on *Cassini* and the reference source. The duration of each scan was typically 50 s on *Cassini* and 60 s on the reference source, but the reference source scan durations were up to 90 s for particularly weak sources. During each epoch we also scheduled a 40 minute block of short scans on tropospheric calibration sources taken from the geodetic block lists.[6]

The signal from *Cassini* is strong, but the phase reference sources are often weak. This is a trade-off to minimize the angular separation between the spacecraft and reference sources. The VLBA sensitivity for continuum sources has improved significantly over the years as the bandwidth of data recording has increased. This has allowed the use of reference sources weaker than 0.1 Jy (see Table 1). Radio sources this weak have only recently been included in the radio source catalogs that define the International Celestial Reference Frame (ICRF; Ma et al. 2009; Fey et al. 2015; P. Charlot et al. 2019, in preparation[7]), and consequently their ICRF positions are usually less well determined than for stronger sources. Continuing VLBI observations to improve and expand the ICRF source catalog will improve the accuracy of weak reference source positions in the future.

3. Data Analysis

Data from the VLBA antennas were cross-correlated by the DiFX software correlator (Deller et al. 2007, 2011) at the Array Operations Center in Socorro, New Mexico. The correlated data and associated calibration information were transferred to the Astronomical Image Processing System (AIPS; Greisen 2003) for editing, calibration, and imaging. The first steps of data analysis in AIPS involved a priori calibration based on recorded system temperatures, antenna gain curves, and corrections for digital sampling effects, parallactic angle, updated Earth orientation parameters, and instrumental bandpass responses. These calibration steps are described in more detail in Beasley & Conway (1995) and Jones et al. (2011).

Additional calibration of signal propagation delays through the ionosphere and troposphere were based on spatial and temporal interpolations of global ionosphere electron content maps derived from Global Navigation Satellite System (GNSS) measurements (Hernandez-Pajares et al. 2009) and tropospheric water vapor derived from rapid VLBI observations of strong radio sources over a wide range of elevations (Mioduszewski & Kogan 2004). These propagation effects vary with time and direction at each telescope, and therefore must be calibrated using near-real-time GPS and delay-versus-elevation measurements. Solar plasma effects could not be explicitly calibrated with our single-frequency-band observations, but should be nearly identical along each line-of-sight pair.

We used AIPS task TECOR to calibrate ionosphere delays based on zenith electron content maps produced by the Jet Propulsion Laboratory (JPL) and archived by NASA's Crustal Dynamics Data Interchange System (CDDIS). TECOR does the interpolations to determine the total electron content along

[6] http://cfa-www.harvard.edu/~reid/atmospheric_delay_calibration.html

[7] See also http://iers.obspm.fr/icrs-pc/newwww/icrf/.

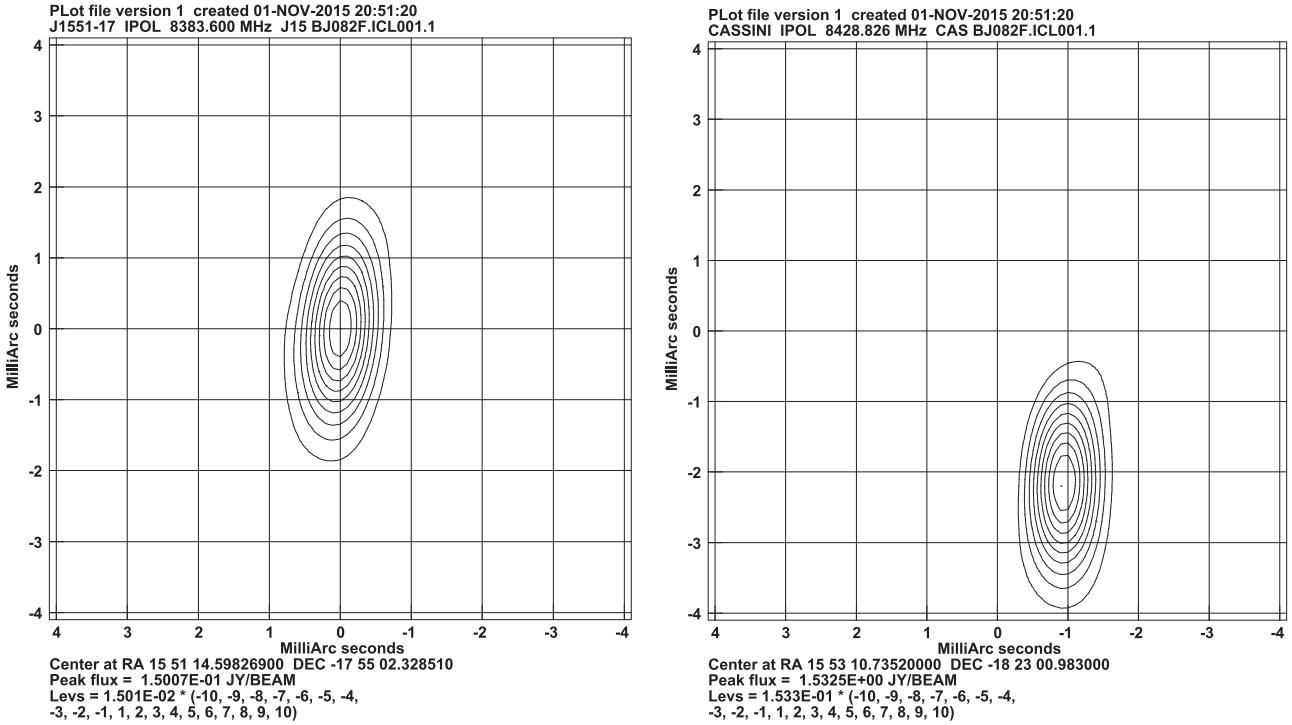

Figure 1. Phase reference source (left) and phase-referenced image of *Cassini* (right) from epoch BJ082F. In both images the contour intervals are 10% of the peak flux density.

each telescope's line of sight during each scan, and calculates the resulting dispersive delays.

Propagation delays due to tropospheric water vapor were calibrated using AIPS tasks MBDLY and DELZN after using a strong source to correct for instrumental delay offsets between IF bands. MBDLY fits multiband delays to the troposphere calibration source scans, which are scheduled to cover a wide range of elevation angles at each telescope over a relatively short time. The multiband delays are read by DELZN and used to calculate residual troposphere (and clock) corrections for each telescope as a function of time. Having nearly simultaneous delays at multiple elevations allows atmospheric effects to be separated from clock errors. We used either two or three polynomial terms for the atmospheric delay fit in DELZN, and two terms for the clock fit.

Calibration of the bandpass response for each telescope was done with AIPS task BPASS using a strong source. Because we generally had good phase stability during the strong source scans we did not need to normalize before determining the bandpass solutions, but we did normalize the amplitudes and zero the average bandpass phases before the solutions were applied to each IF and each antenna.

We produced self-calibrated images of the phase reference sources and phase-referenced images of *Cassini* along with total baseline delays (removing the geometric model used during data correlation). The images were used to check for significant reference source structure and for an initial measurement of the spacecraft offset from the a priori position used during correlation. These a priori positions were obtained from orbit solutions based on Deep Space Network (DSN) tracking and provided by JPL.

Most of our phase reference sources did not show significant extended structure, as one of the selection criteria used was evidence of a highly compact structure. This was determined by examining plots of correlated flux density as a function of projected baseline length, and previous point-like images when available. Data from the USNO radio reference frame image database[8] or DSN radio source catalog observations were used for this purpose.

Figure 1 shows example images of a phase reference source (J1551–1755) and the associated phase referenced image of *Cassini* from epoch BJ082F.

Residual baseline delay corrections derived from the phase-referenced images were included in the total delay data sent to JPL. These total delay values for each baseline, and for both *Cassini* and the reference source, were the primary result from each of our VLBA epochs. Corrections for galactic aberration (Liu et al. 2012) were included, although they are well below our current error levels.

4. Results

4.1. Previous Results

To obtain ICRF-based positions for the Saturn system barycenter at each observing epoch, we combine two independent angular offset measurements. First, our VLBA measurement of the angular offset between a reference source with a known ICRF position and the *Cassini* spacecraft gives us an ICRF position for *Cassini*. Second, the angular offset between *Cassini* and the Saturn system barycenter is determined from a solution for the spacecraft orbit about the planet from Doppler and range tracking by the DSN (Thornton & Border 2000).

The uncertainty in each Saturn ICRF position depends on the precision of our VLBA differential position measurements, the precision of the DSN spacecraft orbit solution, and the accuracy of the assumed phase reference source position.

[8] https://www.usno.navy.mil/USNO/astrometry/vlbi-products/rrfid

Table 2
A Priori Positions of Phase Reference Sources Used for *Cassini* Astrometry

Reference Source	R.A. (J2000)	R.A. Error (mas)	Decl. (J2000)	Decl. Error (mas)	Ref
J0700+1709	07 00 01.525543	0.03	+17 09 21.70131	0.03	ICRF3
J0748+2400	07 48 36.109281	0.03	+24 00 24.10994	0.03	ICRF3
J0931+1414	09 31 05.342427	0.13	+14 14 16.51888	0.23	ICRF3
J1025+1253	10 25 56.285370	0.05	+12 53 49.02192	0.06	ICRF3
J1112+0724	11 12 09.558520	0.12	+07 24 49.11790	0.26	ICRF3
J1127+0555	11 27 36.525544	0.08	+05 55 32.05926	0.15	ICRF3
J1304–0346	13 04 43.642206	0.13	−03 46 02.55080	0.30	ICRF3
J1408–0752	14 08 56.481206	0.03	−07 52 26.66653	0.03	ICRF3
J1434–1146	14 34 21.135858	0.08	−11 46 19.51119	0.18	ICRF3
J1502–1508	15 02 25.01745	0.11	−15 08 52.5192	0.11	BJ082
J1507–1652	15 07 04.786963	0.04	−16 52 30.26715	0.06	ICRF3
J1508–1548	15 08 35.70160	0.11	−15 48 31.5312	0.14	BJ082
J1551–1755	15 51 14.598309	0.13	−17 55 02.32572	0.31	ICRF3
J1608–1625	16 08 07.021395	0.24	−16 25 00.07685	0.54	ICRF3
J1617–1941	16 17 27.093076	0.12	−19 41 32.01477	0.28	ICRF3
J1642–2007	16 42 05.290929	0.18	−20 07 24.84945	0.42	ICRF3
J1700–2610	17 00 53.154064	0.03	−26 10 51.72539	0.03	ICRF3
J1709–1728	17 09 34.34539	0.02	−17 28 53.3651	0.03	GSFC
J1742–1517	17 42 11.66283	0.09	−15 17 29.1585	0.12	JPL

Notes. References for source positions and uncertainties: BJ082 = phase referenced with respect to J1507–1652 in experiment BJ082E. GSFC = Goddard 2016a astrometric solution (https://vlbi.gsfc.nasa.gov/solutions/itrf/2016a/2016a.html). ICRF3 = International Celestial Reference Frame 3 (P. Charlot et al. 2019, in preparation, see also http://iers.obspm.fr/icrs-pc/newwww/icrf/icrf3sx.txt). JPL = Deep Space Network VLBI (Curkendall & Border 2013; Jacobs 2013).

Differential VLBA position measurements can have a precision of less than 0.1 mas, depending on the accuracy of calibration and the angular separation between sources. Our observations, using global total electron content (TEC) maps instead of dual-frequency measurements for ionosphere calibration, and multiple elevation delays and mapping functions instead of water vapor radiometers at each telescope for troposphere calibration, do not reach the highest precision that differential VLBI is capable of. However, the scatter in post-fit position residuals (see Section 5) indicates that our measurement errors are no greater than about 0.2 mas in R.A. and 0.3 mas in decl. for most epochs.

The uncertainty in spacecraft position with respect to Saturn depends on the quality of the final orbit solution produced by DSN tracking. This is typically less than 0.1 mas in sky position and 1 m in range for short-period orbiters, but can be significantly larger for longer spacecraft orbits because the dynamical Doppler signature is smaller (Russell 1970). For *Cassini* the orbit solutions are more complicated due to frequent flybys of the Saturnian moons, and it has not always been possible to determine an accurate error estimate. The spacecraft position uncertainty was 0.2 mas during the 2015 January epoch, which is the largest uncertainty for the mission before the final three epochs. For some epochs the *Cassini* orbit determination may be a dominant error contribution.

For other epochs the uncertainty in the phase reference source position is the dominant contributor to the error budget. Reference sources with large position errors will be included in future VLBI source catalog observations; their improved ICRF positions will directly improve the Saturn system barycenter positions and thus the quality of Saturn's orbit.

4.2. New Results

Since 2015 the VLBA has been able to record data at 2 Gb s^{-1} at each telescope. This increased the continuum sensitivity of the array by a factor of two (or more) over earlier epochs, and therefore allowed angularly closer phase reference sources to be used. We selected reference sources based on flux density (~0.1 Jy or stronger on long VLBI baselines), compactness (point-like images, approximately flat fringe amplitudes versus projected baseline lengths), and the angular distance from *Cassini* (less than 2°.5 whenever possible). However, there were epochs at low galactic latitudes where the nearest usable reference source available was up to 7° away. Table 1 lists our observing epochs since those previously published (Jones et al. 2011, 2015).

The accuracy of reference source positions is being continuously improved with additional VLBI source catalog observations by several international groups. This ongoing observational effort has produced the next generation inertial reference frame, ICRF3 (Malkin et al. 2014; Jacobs 2015; P. Charlot et al. 2019, in preparation[9]). In addition, some optically bright reference sources will have more accurate optical positions from *Gaia* (Gaia Collaboration et al. 2018). For these sources the major uncertainty in radio positions will be from possible offsets in the optical and radio centroids (Petrov & Kovalev 2017; Petrov et al. 2019). Future improvements in reference source positions will allow our VLBI measurements to be reanalyzed to provide even better constraints on Saturn's orbit. Table 2 lists the assumed ICRF positions for the reference sources used.

Note that the position errors included in Table 2 are the published formal errors and may not include all systematic effects. Nevertheless, post-fit residuals indicate that the majority of our reference sources have ICRF positions that are accurate to 0.3 mas or better.

5. Saturn's Orbit

The trajectory of *Cassini* is determined by numerical integration of the equations of motion in a global orbit and

[9] See also http://iers.obspm.fr/icrs-pc/newwww/icrf/.

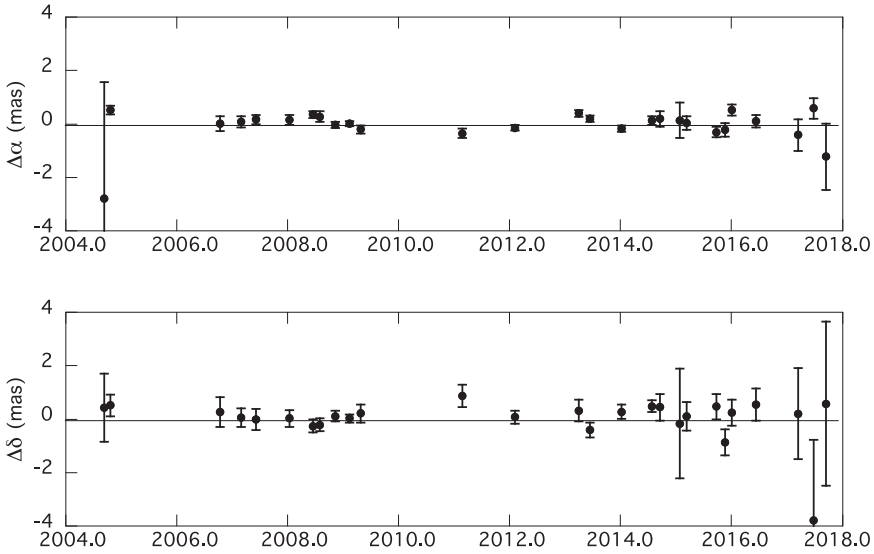

Figure 2. Post-fit residuals of Saturn's orbit fit to VLBA determined positions for the Saturn system barycenter, in R.A. (top) and decl. (bottom). The rms scatter in the residuals is 0.64 mas in R.A. and 0.82 mas in decl. if the two obvious outliers are included, and 0.35 and 0.36 mas if they are excluded.

Table 3
Saturn Barycenter Positions and Uncertainties for Each Epoch Plotted in Figure 2

Observation Epoch	Obs. Time (UTC)	R.A. (h m s)	R.A. Sigma (ms)	Decl. ($d\ ''$)	Decl. Sigma (mas)
2004 Sep 8	18:00	07 43 57.853889	0.290	+21 06 11.47476	1.3
2004 Oct 20	15:00	07 55 53.034197	0.011	+20 38 19.77451	0.4
2006 Oct 11	17:00	09 39 54.457122	0.019	+14 57 55.39369	0.6
2007 Mar 1	07:00	09 31 40.709307	0.014	+16 02 49.54172	0.3
2007 Jun 8	00:00	09 31 40.531530	0.012	+15 59 06.93807	0.4
2008 Jan 12	11:00	10 41 00.483754	0.013	+10 11 48.89103	0.3
2008 Jun 14	02:00	10 22 30.546176	0.008	+11 58 53.88554	0.2
2008 Aug 1	23:00	10 40 08.936950	0.014	+10 12 43.11736	0.2
2008 Nov 11	17:00	11 24 07.553623	0.008	+05 51 34.99287	0.2
2009 Feb 11	14:00	11 27 15.292868	0.006	+05 56 37.40007	0.2
2009 Apr 24	06:00	11 09 02.825585	0.011	+07 52 58.01112	0.3
2011 Feb 21	13:00	13 04 44.278169	0.011	−04 01 53.03484	0.4
2012 Feb 5	12:00	13 52 45.726285	0.007	−08 49 32.02225	0.2
2013 Mar 31	11:00	14 33 46.748594	0.009	−12 17 22.06977	0.4
2013 Jun 14	07:00	14 14 41.930128	0.008	−10 47 07.54172	0.3
2014 Jan 6	18:00	15 15 19.189139	0.008	−15 48 38.31489	0.3
2014 Jul 23	05:00	14 58 34.527332	0.011	−14 35 05.10615	0.2
2014 Sep 16	02:00	15 08 19.987395	0.019	−15 29 37.16794	0.5
2015 Jan 25	14:00	16 04 46.115842	0.044	−18 47 26.10214	2.0
2015 Mar 9	12:00	16 12 32.725953	0.016	−19 01 37.54024	0.5
2015 Sep 21	00:00	15 52 50.087325	0.013	−18 24 05.43685	0.5
2015 Nov 20	00:00	16 17 53.359382	0.017	−19 41 35.27276	0.5
2016 Jan 4	17:00	16 40 03.539512	0.014	−20 31 07.24183	0.5
2016 Jun 9	09:54	16 44 49.784860	0.016	−20 30 11.37936	0.6
2017 Mar 15	15:00	17 47 47.600838	0.040	−22 05 09.34911	1.7
2017 Jun 23	08:23	17 32 43.915344	0.026	−21 56 44.68715	1.0
2017 Sep 11	03:00	17 21 50.890352	0.083	−22 01 05.80935	3.1

gravitational field solution (Jacobson 2006; Antreasian et al. 2007). Figure 2 shows the post-fit residuals of our VLBI-based Saturn system barycenter positions with respect to a fit for Saturn's orbit that is close to that in JPL's DE438 ephemeris (Folkner et al. 2016). Figure 2 covers the full duration of the *Cassini* orbital mission.

The larger uncertainties on the most recent epochs are mainly due to larger uncertainties in the phase reference source positions when weaker reference sources were used, or when larger angular separations between the reference source and *Cassini* had to be used. The reference source positions will improve with time, as described below. In general, the residuals in decl. are larger than in R.A. because Saturn has been at southern declinations during most of the *Cassini* mission, and thus at low southern elevations for the (northern hemisphere) VLBA telescopes. Tropospheric delay calibration errors translate more directly into decl. errors in this geometry. This is particularly true for the Brewster, Washington, VLBA telescope, which provided most of the array's resolution in decl. and at which *Cassini* was observed at much lower elevations during the later years of the mission. *Cassini* and Saturn were at positive declinations during the first few years of

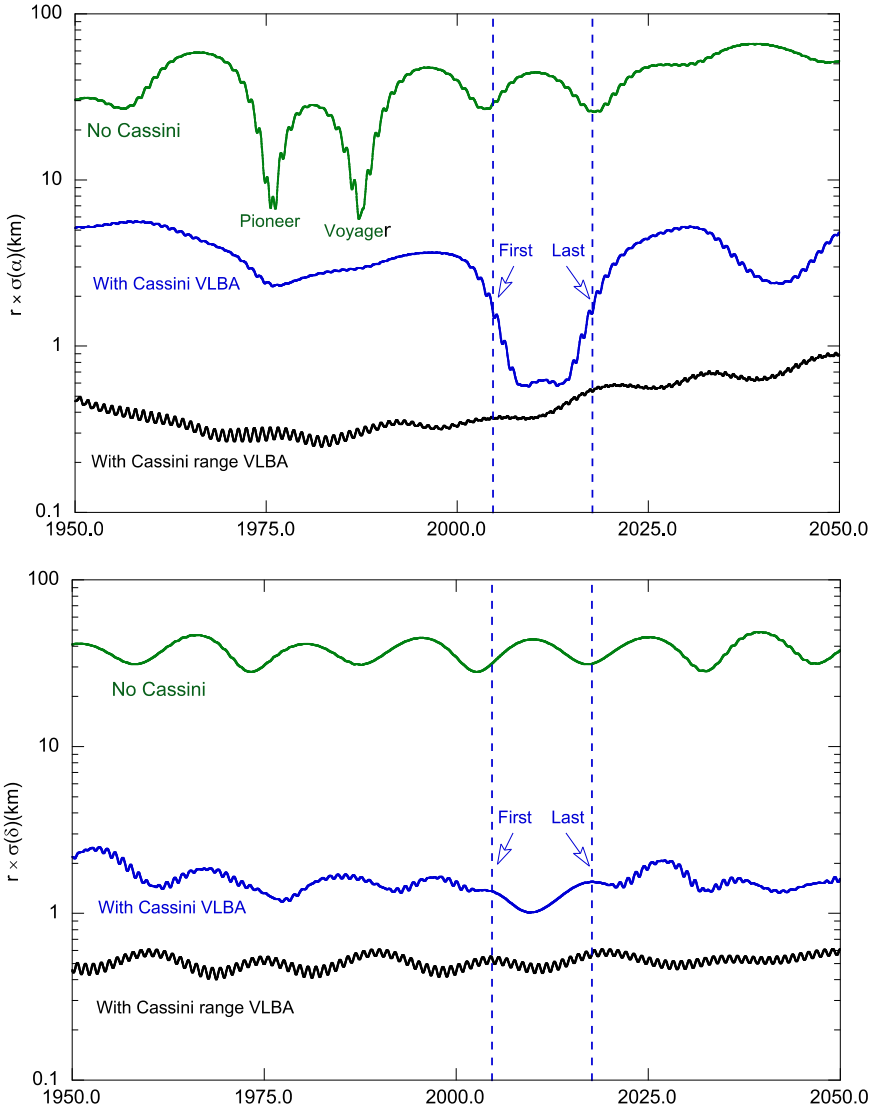

Figure 3. Formal uncertainties in the position of Saturn with respect to Earth in R.A. (top) and decl. (bottom) from 1950 to 2015. The vertical axis is logarithmic on both plots, and the vertical dashed lines indicate the beginning and end of the *Cassini* orbital mission. The bottom curves are based on combining DSN range and VLBA position data during the *Cassini* mission.

the orbital mission, crossed zero decl. in late 2010, and remained at southern declinations for the remaining seven years of the mission.

The rms deviation of the post-fit position residuals is 0.64 mas in R.A. and 0.82 mas in decl. Note that there are two points with unusually large residual offsets: the first epoch in R. A. and the next to last epoch in decl. The first epoch (2004 September 8) occurred during *Cassini*'s initial capture orbit around Saturn, before highly accurate solutions for the *Cassini*–Saturn position offsets were available. The next to last epoch (2017 June 23) occurred during one of the final very low periapse passes of Saturn and there appears to be an unexplained systematic error in the spacecraft orbit during this time. This point was not used in the ephemeris fit. Removing these two epochs results in residual rms values of 0.35 mas in R.A. and 0.36 mas in decl.

A few other points in Figure 2 have larger than average errors. The 2015 January 25 epoch used reference source J1608–1625 that has the largest ICRF position errors of any reference source used for any epoch in both R.A. and decl. The 2017 March 15, June 23, and September 11 epochs all had an unusually large angular separation between the reference source and *Cassini* of nearly 7°. These cases were the result of a lower sky density of suitable reference sources near the galactic plane. The 2017 March 15 epoch also had fewer VLBA antennas producing good data than other epochs, and unusually difficult troposphere delay calibration.

It is likely that ionosphere and troposphere calibration errors are larger for the three final epochs since the larger angular separation will result in less complete cancellation of these effects between the reference source and *Cassini* lines of sight. If the first epoch and the final three epochs are removed, the rms of the remaining 23 epochs is 0.24 mas in R.A. and 0.36 mas in decl. Table 3 lists the Saturn barycenter positions and uncertainties for each epoch plotted in Figure 2. The uncertainties are twice the formal error of Cassini's position relative to Saturn plus the error in the reference source's ICRF position. The Saturn positions are the direction from Earth at observation time to the Saturn system barycentric positions one light-travel time earlier.

Figure 3 plots the uncertainty in the position of Saturn with respect to Earth over a 100 yr period, illustrating the

improvement provided by the VLBA and *Cassini* range measurements.

Our VLBA astrometry provided a large improvement in the orientation of Saturn's orbit during the early years of the *Cassini* mission, while DSN range measurements improved the orbit orientation more near the end of the mission. The formal uncertainties shown in Figure 3 are probably optimistic by about a factor of two, but the dramatic improvement in Saturn's orbit resulting from the *Cassini* mission (combining range and VLBA data) is clear.

Figure 3 shows that the VLBA data improve the accuracy of Saturn's position in R.A. more dramatically than in decl., but the improvement extends farther in time from the VLBA observing period in decl. than it does in R.A. This is caused by the fact that the error in Saturn's R.A. is sensitive to both the orientation of the orbit plane and the shape of the orbit. Range data determine the orbit shape (period, eccentricity, longitude of perihelion) more accurately than VLBI data. Uncertainties in the orbit shape cause uncertainties in R.A. that increase with time. Consequently the Saturn R.A. accuracy degrades rapidly with time if no range data is included with the VLBA data. For decl. the errors are not as sensitive to orbit shape, so the improvement in the orbit orientation (inclination) from VLBA data results in a reduction in decl. error that extends well beyond the VLBA observing period even in the absence of range data.

6. Future Work

The VLBI observing programs that support the ICRF are incorporating higher frequencies that allow higher astrometric accuracy (de Witt et al. 2016; De Witt et al. 2019). These programs will produce more accurate positions for the phase reference sources we have used, allowing a reanalysis of the VLBA data to further improve the planetary ephemeris. The few epochs that used phase reference sources more than 6° from *Cassini* will likely not benefit from improved reference source positions, since systematic errors in ionosphere and troposphere calibration are probably dominant in these cases.

Future VLBI astrometry of spacecraft may be able to utilize 32 GHz downlink signals, which will significantly reduce ionospheric effects, and advanced water vapor radiometers at VLBA sites to improve troposphere calibration. Dual-band observations at 8 and 32 GHz would be particularly desirable for the reduction of residual ionosphere errors.

We are currently applying the same VLBA phase-referenced astrometric techniques to observations of the Juno spacecraft while it orbits Jupiter. In due course we expect to be able to improve the accuracy of Jupiter's orbit to a level similar to the new Saturn orbit determination. At that point two of the four gas giant planets that dominate solar system dynamics will have significantly better orbit determinations.

Eventually orbiting missions to Neptune and Uranus will allow us to improve their orbits as well.

7. Conclusions

We have used the astrometric capabilities of the VLBA to determine accurate ICRF positions of the *Cassini* spacecraft during 22 epochs between 2004 and 2017. Combining these positions with spacecraft ranging and solutions for the orbit of *Cassini* about Saturn provided ICRF positions for the Saturn system barycenter, which in turn were used to improve the parameters of Saturn's orbit about the Sun. The orientation of Saturn's orbit is particularly sensitive to combined astrometric and range constraints, and this has now been determined to an accuracy of 0.25 mas, an order of magnitude improvement over the pre-*Cassini* uncertainty.

We thank the anonymous referee for helpful comments that improved the paper. Part of this research was carried out at the Jet Propulsion Laboratory, California Institute of Technology, under contract with the National Aeronautics and Space Administration. The VLBA is operated by the Long Baseline Observatory, a facility of the National Science Foundation operated under cooperative agreement by Associated Universities, Inc. The National Radio Astronomy Observatory is a facility of the National Science Foundation operated under cooperative agreement by Associated Universities, Inc. Partial support of this research was provided by a grant from the NASA Planetary Astronomy program to the Space Science Institute. This work has made use of the Swinburne University of Technology software correlator, developed as part of the Australian Major National Research Facilities Program and operated under license. We thank E. Fomalont for valuable guidance and technical contributions during the early phases of this work.

ORCID iDs

Robert A. Jacobson https://orcid.org/0000-0002-8844-724X
Jonathan Romney https://orcid.org/0000-0003-4410-5421

References

Antreasian, P. G., Bordi, J. J., Criddle, K. E., et al. 2007, in AIAA/AAS Astrodynamics Specialist Conf., Advances in the Astronautical Sciences Series, Vol. 129, ed. R. J. Proulx, T. J. Starchville, R. D. Burns, & D. J. Scheeres (San Diego, CA: Univelt, Inc.), 21
Beasley, A. J., & Conway, J. E. 1995, in ASP Conf. Ser. 82, Very Long Baseline Interferometry and the VLBA, ed. J. A. Zensus, P. J. Diamond, & P. J. Napier (San Francisco, CA: ASP), 327
Curkendall, D. W., & Border, J. S. 2013, IPNPR, 193, 1
de Witt, A., Bertarini, A., Jacobs, C. S., et al. 2016, in Int. VLBI Service for Geodesy and Astrometry, 2016 General Meeting Proc.: New Horizons with VGOS, ed. D. Behrend, K. D. Baver, & K. L. Armstrong (Greenbelt, MD: NASA), 302
de Witt, A., Gordon, D., Jacobs, C. S., et al. 2019, in Proc. 24th European VLBA Group and Geodesy and Astrometry, ed. R. Haas, S. Garcia-Espada, & J. A. López-Fernández (Madrid: CNIG), P306
Deller, A. T., Brisken, W. F., Phillips, C. J., et al. 2011, PASP, 123, 275
Deller, A. T., Tingay, S. J., Bailes, M., & West, C. 2007, PASP, 119, 318
Fey, A. L., Gordon, D., Jacobs, C. S., Ma, C., Gaume, R. A., et al. 2015, AJ, 150, 58
Folkner, W. M., Park, R. S., & Jacobson, R. A. 2016, JPL Memorandum IOM 392R-16-003
Fomalont, E. 2006, in IVS 2006 General Meeting Proc., ed. D. Behrend & K. D. Baver (Greenbelt, MD: NASA), 307, http://ivscc.gsfc.nasa.gov/publications/gm2006/fomalont.pdf
Gaia Collaboration, Mignard, F., et al. 2018, A&A, 616, A14
Greisen, E. W. 2003, in Information Handling in Astronomy—Historical Vistas, ed. A. Heck (Dordrecht, The Netherlands: Kluwer), 109
Guirado, J. C., Ros, E., Jones, D. L., et al. 2001, A&A, 371, 766
Hees, A., Bailey, Q. G., Le Poncin-Lafitte, C., et al. 2015, PhRvD, 92, 064049
Hernandez-Pajares, M., Juan, J. M., Sanz, J., et al. 2009, JGeod, 83, 263
International VLBI Service for Geodesy and Astrometry, http://ivscc.gsfc.nasa.gov
Jacobs, C. S. 2013, DSN Telecommunications Link Design Handbook, DSN No. 810-005, Module 107B (Pasadena, CA: Jet Propulsion Laboratory) http://deepspace.jpl.nasa.gov/dsndocs/810-005/107/107B.pdf
Jacobs, C. S. 2015, in The Radio-based ICRF: Multi-wavelength Progress, Gaia for AGN and Extragalactic Science (GAGNES) Coll., ed.

B. Rocca-Volmerange, J. Souchay, E. Slezak, & A. H. Andrei (Paris: IAP), 1, www.iap.fr/gagnes/talks/Jacobs_Gagnes.pdf
Jacobson, R. A. 2006, AJ, 132, 2520
Jones, D. L., Folkner, W. M., Jacobson, R. A., et al. 2015, AJ, 149, 28
Jones, D. L., Folkner, W. M., Parks, R. S., et al. 2018, in 2018 IEEE Aerospace Conference (Piscataway, NJ: IEEE), 3.0403, http://ieeexplore.ieee.org/stamp/stamp.jsp?tp=&arnumber=8396396&isnumber=8396361
Jones, D. L., Fomalont, E., Dhawan, V., et al. 2011, AJ, 141, 29
Konopliv, A. S., Yoder, C. F., Myles Standish, E., Yuan, Dah-Ning, & Sjogren, W. L. 2006, Icar, 182, 23
Lazio, T. J. W., Bhaskaran, S., Cutler, C., et al. 2017, in Proc. IAU Symp. 337, Pulsar Astrophysics-The Next 50 Years, ed. P. Weltevrede, B. B. P. Perera, L. L. Preston, & S. Sanidas (Cambridge: Cambridge Univ. Press), 150
Lestrade, J.-F., Rogers, A. E. E., Whitney, A. R., et al. 1990, AJ, 99, 1663
Liu, J.-C., Capitaine, N., Lambert, S. B., Malkin, Z., & Zhu, Z. 2012, A&A, 548, A50
Ma, C., Arias, E. F., Bianco, G., et al. 2009, ITN, 35, 1
Malkin, Z., Jacobs, C. S., Arias, F., et al. 2014, in Proc. Journées 2014 Systems de Reference Spatio-temporels, ed. Z. Malkin & N. Capitaine (St. Petersburg: Pulkovo Observatory), 3
Melbourne, W. G. 1976, SciAm, 234, 59
Mioduszewski, A. J., & Kogan, L. 2004, Strategy for Removing Tropospheric and Clock Errors using DELZN, AIPS Memo, 110, www.aips.nrao.edu/aipsdoc.html
Napier, P. J. 1995, in ASP Conf. Ser. 82, Very Long Baseline Interferometry and the VLBA, ed. J. A. Zensus, P. J. Diamond, & P. J. Napier (San Francisco, CA: ASP), 59
Park, R. S., Folkner, W. M., Jones, D. L., et al. 2015, AJ, 150, 121
Petrov, L., & Kovalev, Y. Y. 2017, MNRAS, 471, 3775
Petrov, L., Kovalev, Y. Y., & Plavin, A. V. 2019, MNRAS, 482, 3023
Porcas, R. W. 2009, A&A, 505, L1
Russell, R. K. 1970, The Deep Space Network, Space Programs Summary 37-61, Vol. II (Pasadena, CA: Jet Propulsion Laboratory), 32
Shin, D., Bagri, D., & Border, J. 2014, IPNPR, 199, 1
Sovers, O. J., Fanselow, J. L., & Jacobs, C. S. 1998, RvMP, 70, 1393
Standish, E. M., & Williams, J. G. 2006, in Explanatory Supplement to the Astronomical Almanac, ed. P. K. Seidelmann (Mill Valley, CA: Univ. Science Books), 305
Thompson, A. R., Moran, J. M., & Swenson, G. W. 2017, Interferometry and Synthesis in Radio Astronomy (3rd ed.; Cham: Springer)
Thornton, C. L., & Border, J. S. 2000, in Radiometric Tracking Techniques for Deep-Space Navigation, ed. J. H. Yuen (Pasadena, CA: Jet Propulsion Laboratory) https://descanso.jpl.nasa.gov/monograph/series1/Descanso1_all.pdf